

Alma Mater Studiorum Università di Bologna  
Archivio istituzionale della ricerca

Dielectric elastomer materials for large-strain actuation and energy harvesting: A comparison between styrenic rubber, natural rubber and acrylic elastomer

This is the final peer-reviewed author's accepted manuscript (postprint) of the following publication:

*Published Version:*

Chen Y., Agostini L., Moretti G., Fontana M., Vertechy R. (2019). Dielectric elastomer materials for large-strain actuation and energy harvesting: A comparison between styrenic rubber, natural rubber and acrylic elastomer. SMART MATERIALS AND STRUCTURES, 28(11), 1-19 [10.1088/1361-665X/ab3b32].

*Availability:*

This version is available at: <https://hdl.handle.net/11585/710433> since: 2019-12-23

*Published:*

DOI: <http://doi.org/10.1088/1361-665X/ab3b32>

*Terms of use:*

Some rights reserved. The terms and conditions for the reuse of this version of the manuscript are specified in the publishing policy. For all terms of use and more information see the publisher's website.

This item was downloaded from IRIS Università di Bologna (<https://cris.unibo.it/>).  
When citing, please refer to the published version.

(Article begins on next page)

This is the final peer-reviewed accepted manuscript of:

Chen, Y. et al., 2019. Dielectric elastomer materials for large-strain actuation and energy harvesting: a comparison between styrenic rubber, natural rubber and acrylic elastomer. *Smart materials and structures*, 28(11), p.114001.

The final published version is available online at:

<https://doi.org/10.1088/1361-665X/ab3b32>

#### Rights / License:

The terms and conditions for the reuse of this version of the manuscript are specified in the publishing policy. For all terms of use and more information see the publisher's website.

This item was downloaded from IRIS Università di Bologna (<https://cris.unibo.it/>)

**When citing, please refer to the published version.**

# Dielectric Elastomer Materials for Large-Strain Actuation and Energy Harvesting: a Comparison Between Styrenic Rubber, Natural Rubber and Acrylic Elastomer

Yi Chen<sup>a</sup>, Lorenzo Agostini<sup>b</sup>, Giacomo Moretti<sup>b</sup>, Marco Fontana<sup>c</sup>, Rocco Vertechy<sup>a\*</sup>

<sup>a</sup>*University of Bologna, Bologna, Italy*

<sup>b</sup>*Scuola Superiore Sant'Anna, Pisa, Italy*

<sup>c</sup>*University of Trento, Trento, Italy*

\*corresponding author ([rocco.vertechy@unibo.it](mailto:rocco.vertechy@unibo.it))

## Abstract

This paper compares the performance of commercially available membranes made of styrenic rubber, natural rubber and acrylic elastomer for dielectric elastomer transducers operating in the large strain regime. Following a detailed description of the adopted experimental set-up and procedures, the results of a comprehensive electro-mechanical characterization of the three materials are reported to highlight the following dependencies: dielectric strength versus stretch, electrical conductivity versus electric field, dielectric constant versus stretch, stress versus stretch and strain rate. This includes the fitting of the experimental data with constitutive equations which provide material property values that can be used for model-based analysis, design and control of dielectric elastomer actuators and generators operating at large levels of strain amplitudes (like, for instance, transducer featuring actuation and generator strains over 100%) or in the presence of large pre-strains (over 100 %). Performance metrics relying on the identified constitutive parameters are introduced in order to discuss the specific pros and cons of the considered elastomers for the development of practical dielectric elastomer transducers.

## 1. Introduction

Dielectric Elastomer Transducers (DETs) are a promising technology for the development of solid-state actuators, generators and sensors [1-4]. DETs comprise one or more sheets of incompressible Dielectric Elastomer (DE) that are sandwiched between compliant electrodes to form a multi-layered electrical capacitor with deformation dependent capacitance [1]. In actuator mode, electrostatic attraction between the oppositely charged electrodes of the DET is used to convert electrical energy into mechanical energy. In generator mode, mechanical energy is converted into electrical energy via the variable-capacitance electrostatic generator

principle. In sensor mode, capacitance measurement is used to infer DET deformation or, indirectly, the applied loads (based on a constitutive model).

Properties of DETs which make them suited for transduction applications are: low specific mass; large deformability; high energy and power densities; moderate or low cost; solid-state monolithic embodiment with no sliding parts; ease of manufacturing, assembling and recycling; good chemical resistance to corrosive environments; silent operation.

Possible applications of DETs are as micro-fluidic pumps and valves [5,6], loudspeakers [7], braille displays [8], tunable lenses [9], soft actuators for robots interacting with humans and the environment [10,11], strain and pressure sensors to monitor body functions [12], and energy harvesters from human motion [13,14] as well as from natural resources (like from ocean waves [15-18, 64, 65]).

Examples of materials used as DEs are acrylic and silicone elastomers [19-22], and nitrile and natural rubbers [23,24]. Examples of materials employed for compliant electrodes are carbon and silver conductive greases [25], the same elastomeric matrices of DEs filled with conductive particles (usually carbon black) [25,26], deposited metallic films [25,27] and highly stretchable ionic conductors made with hydrogels and ionogels [28,29].

The design of effective and optimized DETs requires the knowledge of a set of relevant electromechanical properties of candidate DEs, which makes it possible (1) to appropriately select the most suitable material for the prescribed application and (2) to predict the performance of the resulting transducers as accurately as possible.

To date, several investigations have been conducted on the experimental characterization of DE materials and DET transducers [20,21,22,24,32-35,37-41]. However, the available results typically suffer from the following drawbacks: 1) they do not cover all the electrical and mechanical characteristics of a given material; 2) they are acquired by different research groups and with dissimilar procedures and instrumentations. This makes it difficult to compare the performance of different materials in a specific application.

In this context, this paper reports on a comprehensive experimental characterization that has been performed on three different commercial DE membranes: the THERABAND YELLOW 11726 made of styrenic rubber; the OPPO BAND GREEN 8003 made of natural rubber; the double-sided adhesive acrylic tape VHB 4905 by 3M.

Whereas a number of characterization results by different research groups already exist in the literature for both OPPO BAND GREEN 8003 and VHB 4905 (see for instance in [24]), data for THERABAND YELLOW 11726 are presented and elaborated in this work for the first time.

As regards electrical properties, the dependency of dielectric strength and permittivity of circular specimens on large biaxial deformations are considered along with the dependency of electrical conductivity of similar specimens on applied large electric fields. As regards mechanical behavior, results on the stabilized stress-

strain response of transversally pre-stretched pure-shear specimens under cyclic operation is provided at different deformation rates and for two different levels of strain amplitude.

Data have been acquired for the three materials by using the same experimental set-ups and procedures described in [30] and in operational ranges that are of interest for generators and actuators subject to large stretches. These include: 1) transducers that are pre-stretched anisotropically and with large pre-stretch values [58], so as to set a desired profile of the force-stroke characteristic (at different electric fields); 2) transducers in which the driving actions (i.e., the applied voltage in actuators and the applied mechanical loads in generators) result in large operating strains (namely, actuation and generator strains over 50%). The latter category practically includes those transducers in which a compensation strategy for the DE material stiffness is implemented, which enables the achievement of large operating strokes. In this regard, two types of stiffness compensation strategies exist: 1) static compensation strategies like, for instance, the employment of non-linear biasing elements placed in parallel to the transducer [43, 44, 52, 59, 60] or the connection of the DE membrane perimeter to articulated or flexible frames with suitable kinematics [56, 57]; 2) dynamic compensation strategies like, for instance, the employment of the transducer within a resonant dynamical system, in which the DE material elasticity is counterbalanced by an appropriate amount of mechanical inertia [17-18].

Being focused on large-strain applications, the results presented in this paper may be of limited use for those interested in the analysis and development of actuators and generators operating with small-strain amplitudes (lower than 50%).

Based on performance metrics extrapolated from the acquired experimental data, the paper concludes with a discussion on the potential advantages and disadvantages of each of the considered materials for both actuator and generator applications in the presence of large applied strains.

Although they are among the most promising candidates for DE transducer application, this work does not take into account silicone elastomers (such as the ELASTOSIL® Film 2030 by Wacker), since the thin film carbon grease electrodes used here for dielectric constant and electrical conductivity measurements are not compatible with such materials. Detailed characterization of the ELASTOSIL® Film 2030 by Wacker with screen-printed electrodes made with a carbon black silicone elastomer mixture can be found in [61-63].

## **2. Methodology**

This section describes the experimental set-ups and procedures that have been used for determining the electromechanical properties of the three considered DE membranes.

For each DE membrane under investigation, the different characterization tests have been conducted on the same batch of material.

Specimens of THERABAND YELLOW 11726 and OPPO BAND GREEN 8003 materials are prepared from the virgin band as provided by the manufacturer. Specimens of VHB 4905 are prepared by first laminating (thereby, gluing) three virgin pieces of tape one on top of the other to obtain a three-layered membrane. This has been done for the following two reasons: 1) in a number of practical DET applications, the VHB 4905 is used in the form of laminates made by two/three layers of the base material [17,18, 52-54]; 2) to obtain specimens with similar thickness in the conditions where THERABAND YELLOW 11726 and OPPO BAND GREEN 8003 feature an equi-biaxial stretch equal to 2 and VHB 4905 features an equi-biaxial stretch equal to 5, which correspond to intermediate stretches within the operational ranges considered in this work for electromechanical testing.

Similar to [30], specimen pre-stretch is performed manually by deforming a pattern, drawn on the membrane with a 0.1 mm marker, to the external boundary of a rigid annular frame featuring a larger similar shape. For all the considered pre-stretches, the frame external boundary is a circle with 150 mm diameter in case of electrical test specimens, and a rectangle with 200 mm and 100 mm edges in case of mechanical test specimens; the initial shape sizes drawn on the membranes are adjusted according to the desired values of pre-stretch. Correctness and uniformity of the obtained pre-stretch inside the active specimen area (either circular or rectangular) is checked by verifying the final straightness and separation of the lines initially drawn inside the undeformed pattern with known spacing [30]. Obtained pre-stretch values are calculated after clamping of the membrane to the frame by taking the ratio between the average length of the diameter/edge of the deformed pattern and the average diameter/edge of the undeformed pattern drawn on the membrane. More specifically: length measurements of pattern diameter/edge are taken with a digital caliper with 0.01 mm accuracy; ten measurements are taken along different lines on the membrane; stretching is considered acceptable only if the measurements taken along the different lines do not differ by more than 1 mm; if acceptable, the average of the ten measurements is finally taken as the length of diameter/edge which is then used to calculate pre-stretch. Each experiment has been conducted in a laboratory environment, with a temperature of around 25 °C and a relative humidity of around 60%. Although the electromechanical properties of DEs are known to be affected by temperature, humidity and other environmental factors, the dependency of material characteristics on these effects is not considered in this work.

## ***2.1 Measurement of membrane thickness***

Film thickness has been measured in the unstretched configuration via a high-accuracy CCD laser displacement sensor (Keyence LK-G152); the thickness of the stretched specimens is estimated from that measured in the un-stretched configuration via volume conservation. As shown in Figure 1, tests are performed with the DE membrane specimen interposed between a base flat circular plate and a calibrated disc (made of brass, 50 mm in diameter and 10 mm in height).

In the set-up, the laser is kept fixed and is used to measure the distance of the same central point of the calibrated disc both in the presence and in the absence of the DE material under test. Membrane thickness is then estimated as the difference between these two measures. Correctness and repeatability are verified by repeating the measurements five times on the same specimen and by checking that the acquired values do not differ by more than 3 %; then, the average value is taken as the membrane thickness estimate,  $t$ .

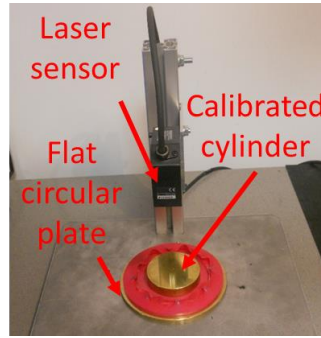


**Figure 1: Set-up for membrane thickness measurement [30]**

Although the use of a calibrated cylinder does not make it possible to measure the membrane thickness locally, the set-up considered here enables to reduce the errors due to imperfect contact between DE membrane and base plate, as well as to imperfect light reflection by the DE membrane (that is likely to be different from a material to one another due to different specimen thickness, roughness and colour). For the considered laser sensor and DE materials, these two issues made indeed it difficult to obtain consistent results with the laser profilometry method suggested in [31].

## ***2.2 Measurement of membrane dielectric strength***

Dielectric strength measurement is performed with unequal cylindrical metallic electrodes with a set-up similar to those suggested in the standards IEC 60243-1 and ASTM D149 for thin films and laminates.

As shown in Figure 2, a cylinder 25 mm in both diameter and height is used as the high voltage electrode, whereas a cylinder 150 mm in diameter and 10 mm in height is used as the ground electrode. Both cylinders are made of brass and with the edges rounded to give a radius of 3 mm; they are arranged coaxially within 2 mm. The cylinder surfaces that are in contact with the membrane are polished and free from irregularities resulting from previous testing. To ensure safety and to limit current dispersions through the surrounding air, the HV electrode is fully embedded in a plastic cylindrical receptacle (constituted by two parts made in Delrin®) that closes onto the DE membrane specimen. This protects the HV electrode from the user's touch

and interrupts the air path to the ground electrode. To limit the exposed metal surface, the bottom face of the ground electrode is embedded in a Delrin® frame.

As for the power, control and measurement electronics: 1) the electric potential difference is provided to the electrodes via a Direct Current (DC) High Voltage (HV) power supply (Untravolt 40A24-P30-C); 2) the connection between HV supply and electrodes is made with double-insulated HV cables; 3) the input voltage is commanded to the HV supply either manually or automatically via a signal generator (ISO-TECH GFG 2004); 4) the electric potential difference commanded and generated by the HV supply are logged automatically to a PC via a USB-based oscilloscope (PicoScope 2202). This set up enables to test DE membrane specimens with maximum electric potential difference selectable in the range from 0 to 40kV, and to obtain breakdown voltage (and thus, dielectric strength) measurements with a resolution equalling 0.8 % of the selected full scale.

For each specimen under test, electric potential difference is applied between the electrodes according to a short-time (rapid-rise) test; that is: voltage is raised from zero at a uniform rate until breakdown occurs, with the rate of rise chosen among 0.5 kV/s, 2 kV/s and 5 kV/s to guarantee the breakdown to occur between 10 s and 20 s. After rupture, the breakdown voltage,  $V_{BD}$ , is extracted from the acquired data and the dielectric strength of the tested specimen is estimated as

$$E_{BD} = V_{BD}/t. \quad (1)$$

To assess any dependency of dielectric strength on strain [32-35], each of the considered materials is here tested at different levels of equi-biaxial deformation.

Since dielectric breakdown in polymers is known to be a stochastic process [31,36], seven specimens are tested for each material and level of deformation.

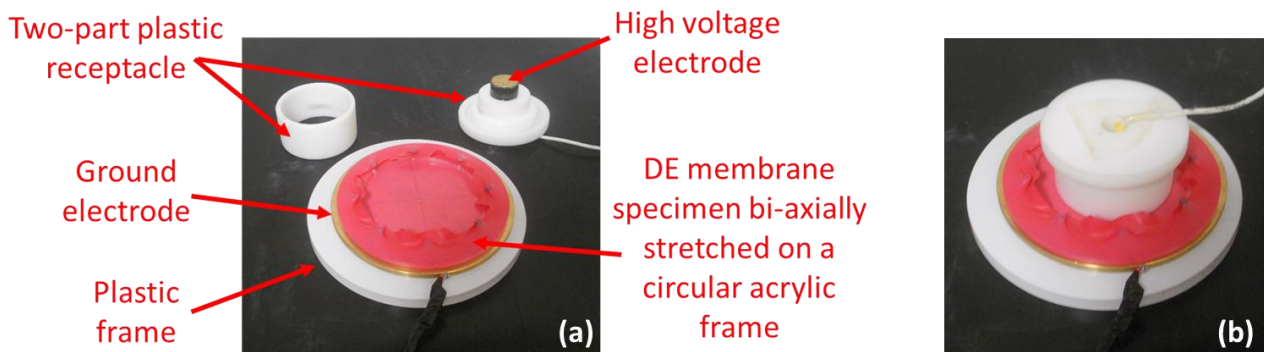


**Figure 2: Electrode set-up for membrane dielectric strength measurement [30]: a) exploded view; b) assembled view**



In contrast with [31], unequal cylindrical electrodes have been preferred here to hemispherical (or spherical) and plate electrodes in order to test on larger volumes of materials, which typically provides more conservative and repeatable values that are closer to those experienced in practical applications. In contrast with the IEC 60243-1 and ASTM D149 standards, the ground electrode of the unequal cylinders set-up is chosen larger than the suggested value (150 mm vs 75 mm) so as to support over their entire area DE membrane specimens that are stretched onto circular frames. This is important since each of the considered materials is here tested at different levels of equi-biaxial deformation in order to assess any dependency of dielectric strength on strain [32-35].

### ***2.3 Measurement of membrane electrical conductivity***

Volume conductivity measurement is performed on the electrode set-up shown in Figure 3 which comprises: 1) the DE membrane under test; 2) an outer plastic frame made of two identical Delrin® rings, each featuring 130 mm internal diameter, 155 mm external diameter and 3 mm thickness, which is used to keep the DE membrane in a pre-stretched state at opposite sides; 3) two identical circular carbon grease (MG Chemicals 846) electrodes with 80 mm diameter that are applied on the opposite sides of the DE membrane after pre-stretch; 4) an inner plastic frame made of two identical Delrin® rings, each featuring 80 mm internal diameter, 120 mm external diameter and 3 mm thickness, which is used to confine the carbon grease electrodes within the prescribed 80 mm diameter; 5) two copper strips for electrical instrumentation connection that are placed at opposite sides in contact with the corresponding carbon grease electrodes and bonded to the inner ring; 6) two insulation layers made of an acrylic tape (VHB 4905 by 3M) located at opposite sides (also embedding the wires of the electrical instrumentation) which are used to minimize spurious resistance paths (both in air and over the surfaces of DE membrane and frames) from HV to ground electrodes and to protect the HV electrode from the user's touch. The same acrylic tape is also used at the interfaces of the Delrin® rings (of both inner and outer frames) with the DE membrane to promote adhesion and insulation.

Electrical conductivity is measured at high voltage by connecting the sample electrodes to the same power, control and measurement electronics described in Section 2.2 and shown in Figure 2.b, with the addition of a pico-amperometer (Keithley 6485 Picoammeter) that is placed between the ground of the DE membrane specimen and the ground of the HV power amplifier. A 1 M $\Omega$  resistor is also connected in series to prevent damage by current or voltage surges in case of electric breakdown of the DE specimen. This set up enables to measure leakage currents across the DE specimen up to 20 mA (although usually employed in the range from 20  $\mu$ A to 0.1 nA).

For each specimen under test, electric potential difference is applied step-by-step, with electric field increments of about 10 MV/m and a hold-time of about 60 s for each voltage level for proper material electrification (namely, for the current to settle after its asymptotic decay due to dielectric absorption and the sweep of mobile ions to the electrodes). At the completion of the test, the steady state values of the current attained at the end

of each step,  $I_L(E)$ , are extracted and the electrical conductivity at a given level of applied electric field,  $E$ , is estimated as

$$\kappa(E) = I_L(E)/(A \cdot E), \quad (2)$$

where  $A$  is the electrode area.

To assess repeatability, tests are performed on three nominally identical specimens of the same membrane. The results are then used to compute mean value and standard deviation.

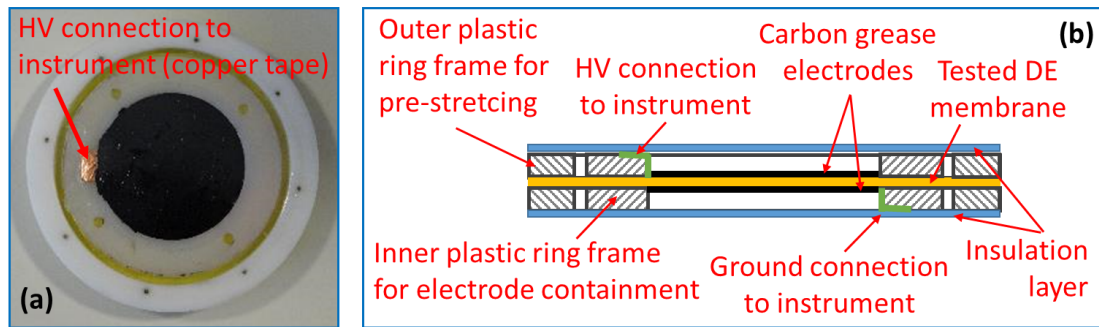


**Figure 3: Electrode set-up for membrane dielectric constant measurement**

In this study, thin film electrodes made with carbon grease are used in place of other electrode systems, like those suggested in the standard ASTM D257, for the following reasons: 1) rigid metallic electrodes like those used for dielectric strength measurements cannot get into intimate contact with the DE membrane under test and, thus, perform worse in all parameter estimations that involve the computation of the ratio of a measured quantity and the specimen area; 2) sprayed and evaporated metal electrodes do not adhere satisfactorily to the styrenic rubber membrane; 3) metal foil electrodes are not adequate for thin membranes like those considered here; 4) carbon grease electrodes are expected to provide electrical property values that are closer to those experienced in many practical investigations, since carbon grease is the most employed material for laboratory prototyping of DETs based on the commercial elastomer films investigated here; 5) carbon grease enables easier and faster preparation of large quantities of specimens.

Being compatible with the three considered DE membrane materials, the use of carbon grease electrodes is not expected to have a significant influence on the electrical properties measured in this work. This choice, however, did not make it possible to test silicone elastomers due to chemical incompatibility. In the future, investigations will have to be performed to find a thin film electrode formulation that is suitable for electrical conductivity testing of a wide variety of DE materials that also include silicone elastomers, as well as to assess the influence of specific electrode formulations on measured electrical properties.

Worth to be mentioned: the considered set-up only uses two electrodes. That is, it does not comprise a third guard electrode as suggested in the standard ASTM D257 to intercept all stray currents that may introduce measurement errors. Here, the guard electrode has been omitted since two insulation layers already exist in the set-up which brake almost any undesired path of conduction between HV electrode and ground electrode (see Figure 3).

## 2.4 Measurement of membrane dielectric constant

Dielectric constant measurement is performed on the same set-up shown in Figure 3 with a LCR bridge (Hameg Instruments LCR meter HM 8118) connected to the specimen electrodes in place of the electronics equipment employed in the previous measurements. This set-up enables the measurement of capacitance values in the range from 0.01 pF to 100 mF, with test frequency, alternate current signal level and bias voltage selectable in the ranges from 20 Hz to 200 kHz, from 50 mV<sub>RMS</sub> to 1.5 V<sub>RMS</sub>, and from 0 V<sub>DC</sub> to 5 V<sub>DC</sub>, respectively.

Each specimen is tested with the LCR meter at 20 Hz with a 5 V<sub>DC</sub> biased alternate current signal having 1.5 V<sub>RMS</sub> root-mean-square magnitude. Once stabilized, the capacitance reading,  $C$ , of the instrument is taken and the relative dielectric constant of the DE membrane,  $\epsilon_r$ , is estimated as

$$\epsilon_r = C \cdot t / (A \cdot \epsilon_0), \quad (3)$$

where  $\epsilon_0$  is the vacuum permittivity ( $\epsilon_0 = 8.8541 \cdot 10^{-12}$  F/m).

To assess any dependency of the dielectric constant on strain [32,33,37,38], each of the considered materials is here tested at different levels of equi-biaxial deformation.

To assess repeatability, measurements are performed on three nominally identical specimens for each testing condition (material and level of stretch). The results are then used to compute mean value and standard deviation.

The following is worth to be mentioned:

- As done for conductivity measurement, carbon grease electrodes have been preferred here to other electrode systems, like those suggested in the standard ASTM D150 and in [31]. The reasons are the same as those provided in Section 2.3.
- In evaluating the DE membrane capacitance value, no correction factor for the stray field at the edge has been applied; in fact, for the large diameter electrodes employed in the set-up, the ratio of fringing capacitance (estimated as per standard ASTM D150 and [39]) and measured capacitance is always less than 2 % for any of the tested specimens.
- Although materials should be tested as close as possible to operating situations, similarly to [32,33,37,38] measurements are performed here at low values of the electric fields, since this is expected to provide

dielectric constant values that apply well also when the material is subjected to high electric fields [17, 18]. Nonetheless, since only a few results exist on the measurement of dielectric constant at high electric field levels, some of them providing different values than those measured at low electric field [17, 33, 55], future studies are required to assess the dependency of the dielectric constant on the electric field in different DE materials.

## 2.5 Measurement of membrane stress-strain response

The mechanical response of the considered DE materials is determined by testing transversally pre-stretched pure-shear specimens with a commercial tensile stage (Galdabini SUN 500). As shown in Figure 4, the adopted pure-shear specimens feature a longitudinal length in the unstretched state equal to 10 mm and a transversal length in the clamped state equal to 200 mm (where longitudinal and transversal respectively mean parallel and normal to the motion direction imposed by the tensile stage).

In this study, each specimen under tests is cycled 10 times between the same deformation limits to remove Mullins effect, which disappears between the sixth and the seventh cycle for the considered materials. The last loading-unloading cycle is then taken as the stabilized response of the specimen.

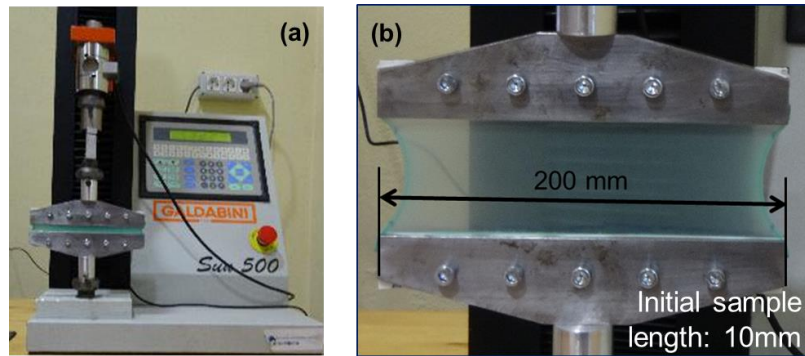


**Figure 4: Set-up for membrane stress-strain response measurement**

To investigate strain-rate dependencies of the mechanical response, each specimen is tested at the following five different strain-rates:  $0.004 \text{ s}^{-1}$ ,  $0.08 \text{ s}^{-1}$ ,  $0.4 \text{ s}^{-1}$ ,  $0.8 \text{ s}^{-1}$  and  $1.2 \text{ s}^{-1}$ .

To investigate dependencies of the mechanical response on the applied level of strain, each specimen is also tested at two different deformation amplitudes:

- 1) Large Stroke: the maximum deformation level is set at 90 % of the elongation at break limit of the considered material, whereas the minimum deformation level is set as the value at null mechanical stress for the cycle performed at a strain rate of  $0.004 \text{ s}^{-1}$ .
- 2) Intermediate Stroke: the strain amplitude is decreased and the deformation range is adjusted so as to get the most effective response from the material, which compromises between minimal loss of tension during maximal electrical activation and reduced viscous losses during cyclical deformation.

As compared to the procedure suggested in [31], here the pure-shear specimens of each of the considered materials are pre-strained in the transversal direction to a value,  $\lambda_{2p}$ , which is expected to provide experimental data that are more suitable for the study of DE generators and actuators operating with large strain amplitudes or subject to large pre-stretches. Moreover, a larger height-to-width ratio (20 instead of 10) is employed to obtain results that better approximate the response of ideal pure-shear specimens, especially at the larger levels of transversal and longitudinal deformation.

### **3. Results**

This section reports the results obtained by testing the three considered commercial DE membranes with the set-ups and procedures described in the previous sections.

#### ***3.1 Measurement of membrane thickness***

Measurement of membrane thickness,  $t$ , provided the following outcomes:

- a mean value of  $293 \text{ }\mu\text{m}$  with a standard deviation of  $5.46 \text{ }\mu\text{m}$  for the samples made of the styrenic rubber band THERABAND YELLOW 11726;
- a mean value of  $224 \text{ }\mu\text{m}$  with a standard deviation of  $3.85 \text{ }\mu\text{m}$  for the samples made of the natural rubber band OPPO BAND GREEN 8003;
- a mean value of  $1492 \text{ }\mu\text{m}$  with a standard deviation of  $15.96 \text{ }\mu\text{m}$  for the samples made of the double-sided pressure-sensitive acrylic tape VHB 4905 (obtained through the lamination of 3 layers of virgin tape).

Since VHB 4905 is sticky and provided with a native paper liner, thickness estimation for this material has been performed with the same procedure described in Section 2.1, but in the following indirect manner: 1) the thickness of the specimen is measured without removing the liner; 2) the liner is removed from the specimen and its thickness measured; 3) specimen thickness is then obtained as the difference of these two measures.

### 3.2 Measurement of membrane dielectric strength

The experimental results of the dielectric strength tests conducted on the considered DE membranes are reported in Figures 5-7 with circle markers. In particular:

- Figure 5 reports the electrical breakdown data acquired on the THERABAND YELLOW 11726 membrane tested at the following three levels of equi-biaxial stretch ( $\lambda$ ): 1, 2.04, 3.12.
- Figure 6 reports the electrical breakdown data acquired on the OPPO BAND GREEN 8003 membrane tested at the following five levels of equi-biaxial stretch ( $\lambda$ ): 1, 1.5, 2, 2.5, 3.
- Figure 7 reports the electrical breakdown data acquired on the VHB 4905 membrane tested at the following four levels of equi-biaxial stretch ( $\lambda$ ): 2, 3, 4, 5.

As shown, identical specimens subjected to the same testing condition (type of material and level of strain) fail at different values of the applied electric field, with the spread of the breakdown data increasing significantly with the level of the applied equi-biaxial stretch. The spread of the breakdown data is quite similar for THERABAND YELLOW 11726 and OPPO BAND GREEN 8003, and smaller for VHB 4905.

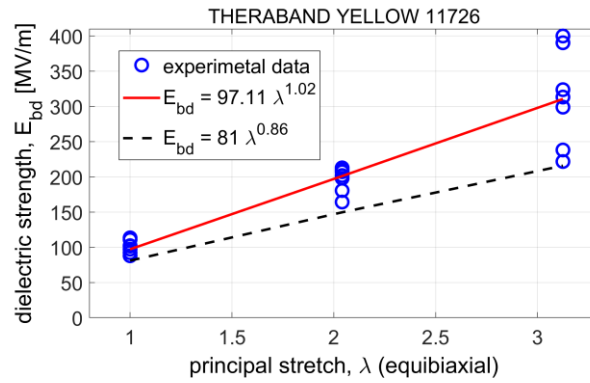


**Figure 5: Dielectric strength vs. stretch correlation for THERABAND YELLOW 11726: experimental data (circles); power law fitting of mean values (red solid line); 90 % reliability power law estimate (black dashed line)**

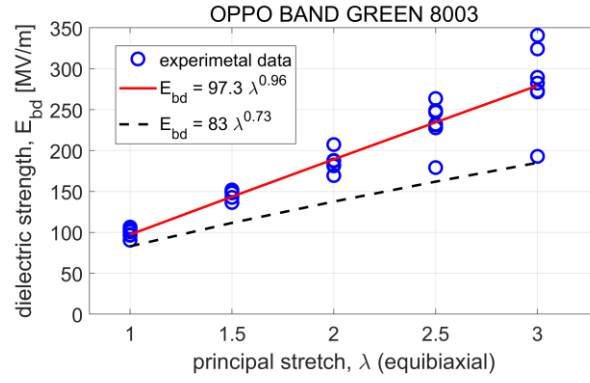


**Figure 6: Dielectric strength vs. stretch correlation for OPPO BAND GREEN 8003: experimental data (circles); power law fitting of mean values (red solid line); 90 % reliability power law estimate (black dashed line)**

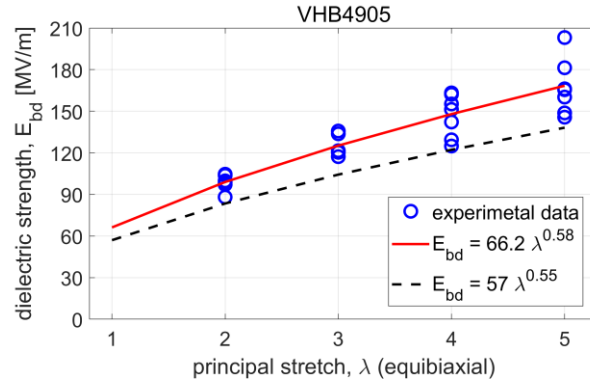


**Figure 7: Dielectric strength vs. stretch correlation for VHB 4905: experimental data (circles); power law fitting of experimental data (red solid line); 92 % reliability power law estimate (black dashed line)**

Despite the increasing spread of the acquired data, breakdown strength resistance of every material is shown to improve markedly with strain. To quantify this increase, the followings have been determined and reported for each material in the respective figures:

- fitting of the experimental data with a power-law in the form

$$E_{BD} = E_0 \cdot \lambda^r \quad (4)$$

(where  $E_0$  and  $r$  are constitutive material parameters, see [24,32], whose fitted values are reported in Table 1), plotted with a solid red line, which represents the mean dielectric strength of the considered material;

- the lower-bound power-law, having the same form

$$\underline{E}_{BD} = \underline{E}_0 \cdot \lambda^{\underline{r}} \quad (5)$$

(where  $\underline{E}_0$  and  $\underline{r}$  are material parameters whose fitted values are reported in Table 1) and plotted with a dashed black line, which represents a limiting threshold not to be exceeded if one wants to guarantee a probability of failure of less than 8% (that is, a reliability higher than 92 % as per IEC 62539).

Property	THERABAND™ YELLOW 11726	OPPO BAND™ GREEN 8003	VHB™ 4905
Unstretched dielectric strength $E_0$ (average) [MV/m]	97.1	97.3	66.2
$\underline{E}_0$ (92 % reliability) [MV/m]	81	83	57
Strengthening exponent $r$ (average)	1.02	0.96	0.58
$\underline{r}$ (92 % reliability)	0.86	0.73	0.55
Dielectric constant $\epsilon_r$	2.72	2.74	4.14
Conductivity at low field (@ $E = E_B$ ) $\kappa_0$ [pS/m]	0.064	0.055	0.57
Conductivity exponential law parameter $E_B$ [MV/m]	56	39	40
1 <sup>st</sup> modulus of the Gent-Gent model $\mu$ (@ $0.4s^{-1}$ ) [KPa]	204.23	496.86	16.92
Chain extensibility limit of the Gent-Gent model $J_m$ (@ $0.4s^{-1}$ )	33.9	538	138.8
2 <sup>nd</sup> modulus of the Gent-Gent model $C_2$ (@ $0.4s^{-1}$ ) [KPa]	185.93	183.80	0.004
Infinitesimal initial shear modulus $\mu_0 = \mu + 2C_2/3$ (@ $0.4s^{-1}$ )	328.18	619.39	16.92
Hysteresis loss $\eta$ (@ $0.4s^{-1}$ , for large strokes) [%]	8.99	21.21	14.64
$\eta$ (@ $0.4s^{-1}$ , for intermediate strokes) [%]	9.4	3.53	11.07

**Table 1: Measured electrical and mechanical material properties of THERABAND YELLOW 11726, OPPO BAND GREEN 8003 and VHB 4905**

Figures and table highlight the following:

- THERABAND YELLOW 11726 and OPPO BAND GREEN 8003 behave quite similarly (the respective parameters  $E_0$ ,  $r$ ,  $\underline{E}_0$  and  $\underline{r}$  are indeed very close), with the former performing slightly better;
- VHB 4905 is the material with worst dielectric strength resistance.



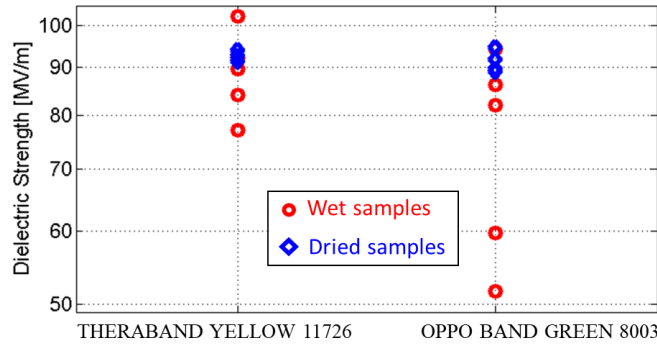


**Figure 8: Dielectric strength for wet (red circle markers) and dried (blue diamond markers) specimens: THERABAND YELLOW 11726 (data on the left) vs. OPPO BAND GREEN 8003 (data on the right) [66]**

The considered styrenic and natural rubber membranes have a similar dielectric strength resistance only if specimens do not come into contact with water. In fact, while immersion into water causes a significant reduction in dielectric strength for OPPO BAND 8003, only a minor variation occurs in the response of THERABAND YELLOW 11726. This is shown in Figure 8, which reports the breakdown data for unstretched membranes that were immersed into water for two days and then tested in the following conditions:

- Wet state (red circle markers), where the samples have been dried with a towel for a few minutes and left for 1 hour at room temperature;
- Dried state (blue diamond markers), where the samples have been dried in an oven at 40 °C for 2 hours.

As it can be seen, in wet state the spread of the breakdown data increases and its average shifts downward; with the spread and shift being larger for the OPPO BAND 8003. This reduction is however only temporary; upon drying, both materials indeed regain an average dielectric strength higher than 90 MV/m (though to an average value of around 93 MV/m that is slightly lower than those reported in Table 1 for specimens that did not get in contact with water). As a possible motivation, the described effect could be due to the water adsorption/permeability of the considered materials that is larger for natural rubber than for styrenic rubber.

As compared to other results existing in the literature, the findings obtained here are in line with those described in [24] and [32], which report  $E_0 = 97$  MV/m and  $r = 0.99$  for the OPPO BAND GREEN 8003 and  $E_0 = 69$  MV/m and  $r = 0.54$  for the VHB 4910 (a tape that has the same formulation of the VHB 4905 and that is just twice in thickness) for experimental data acquired with stamp electrodes embedded in epoxy resin.

### 3.3 Measurement of membrane electrical conductivity

The experimental results of the electrical conductivity tests performed on the considered DE membranes are reported in Figures 9-11. In particular:

- Figure 9 and 10 report the electrical conductivity data respectively acquired on the THERABAND YELLOW 11726 membrane and on the OPPO BAND GREEN 8003 membrane tested at an equi-biaxial stretch of  $\lambda = 2$  (thus, with thicknesses of about 73  $\mu\text{m}$  and 56  $\mu\text{m}$ , respectively).
- Figure 11 reports the electrical conductivity data respectively acquired on the VHB 4905 membrane tested at an equi-biaxial stretch of  $\lambda = 5$  (thus, with a thickness of about 59  $\mu\text{m}$ ).

These levels of stretch have been selected since they lie in the middle of the operational range that is expected for the considered membranes and to provide specimens with comparable thickness (thus, geometrically similar) despite different in material.

In the figures, blue dot markers represent the average over the measurements performed on the three specimens tested at the same conditions, with the blue error bar representing their standard deviation.

As shown, average and standard deviation values increase with the applied electric field irrespective of the considered material.

To quantify the dependency of conductivity with the applied electric field, fitting of the experimental data with an exponential law in the form

$$\kappa = \kappa_0 \cdot \exp(E/E_B) \quad (6)$$

(where  $\kappa_0$  and  $E_B$  are the material parameters to be determined, see [40]) has been performed. For each material, curve fits are plotted in the respective figures with a dashed red line, whereas fitted parameters are reported in Table 1 for comparison.

The figures highlight the following:

- The conductivities of THERABAND YELLOW 11726 and OPPO BAND GREEN 8003 are in the same order of magnitude, with the former performing better from moderate to high electric field levels. In particular, THERABAND YELLOW 11726 is characterized by a slightly larger conductivity at low electric fields (it features a  $\kappa_0$  parameter that is 16 % larger); OPPO BAND GREEN 8003 is instead more sensitive to electric field variations (it features an  $E_B$  parameter that is 30 % smaller).
- VHB 4905 is rather dissipative; its electrical conductivity is one order of magnitude larger than that of the other two materials, mostly due to a large value of  $\kappa_0$  (8.9 times larger than that of THERABAND YELLOW 11726 and 10.3 times larger than that of OPPO BAND GREEN 8003).

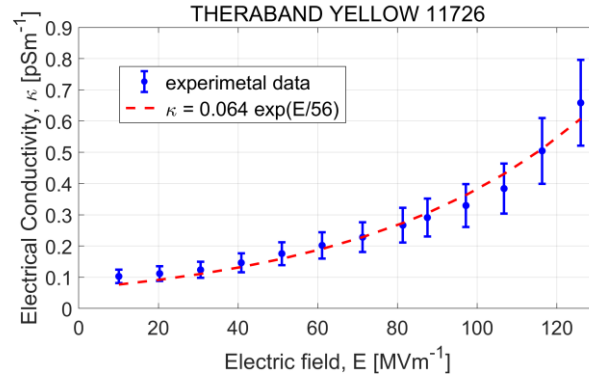


**Figure 9: Electrical conductivity vs. electric field for THERABAND YELLOW 11726 with an equi-biaxial stretch of  $\lambda = 2$ : experimental data (blue dot marker with errorbar); exponential law fitting (red dashed line)**

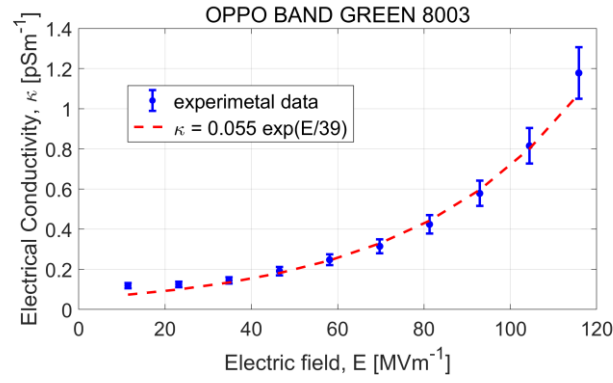


**Figure 10: Electrical conductivity vs. electric field for OPPO BAND GREEN 8003 with an equi-biaxial stretch of  $\lambda = 2$ : experimental data (blue dot marker with errorbar); exponential law fitting (red dashed line)**

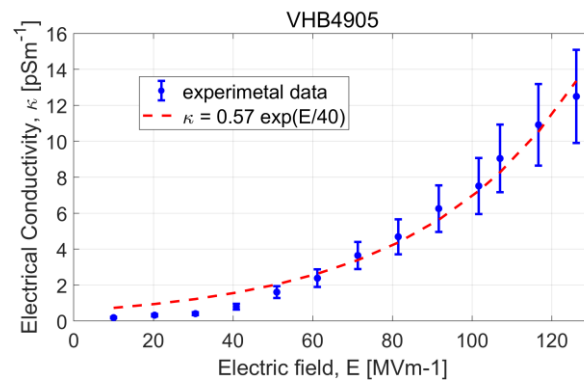


**Figure 11: Electrical conductivity vs. electric field for VHB 4905 with an equi-biaxial stretch of  $\lambda = 5$ : experimental data (blue dot marker with errorbar); exponential law fitting (red dashed line)**

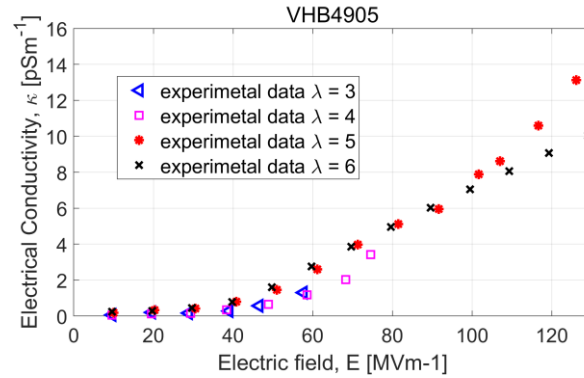


**Figure 12: Electrical conductivity vs. electric field for VHB 4905: results comparison for specimens tested at different levels of equi-biaxial stretch ( $\lambda$ )**

Each of the Figures 9-11 reports data acquired on specimens made of the same material and subjected to the same level of stretch. To verify the possible dependency of the electrical conductivity on mechanical strain, tests have been additionally performed on four specimens of VHB 4905 subjected to four different stretches ( $\lambda$ ): 3, 4, 5, 6. Results are reported in Figure 12 with different markers, which show a rather limited dependency of electrical conductivity on mechanical strain.

As compared to other results existing in the literature, the findings reported here for VHB 4905 are in line with those described in [41] and obtained for the same material but with samples having different geometry (namely, expanding circles with 25 mm initial diameter). Considering indeed the data reported in [41] for an electric field equal to 125 MV/m, one can estimate an average conductivity of  $\kappa(E = 125 \text{ MV/m}) \approx 10.17 \text{ pS/m}$  evaluated over nine nominally identical specimens, with maximum and minimum values equalling 50 pS/m and 5 pS/m (the smallest value being far away from the others, for which it may be considered as an outlier).

### 3.4 Measurement of membrane dielectric constant

The experimental results of the tests conducted for assessing the dielectric constant of the considered DE membranes and its possible dependency on the applied strain are reported in Figures 13-15. In particular:

- Figure 13 and 14 report the dielectric constant data respectively acquired on the THERABAND YELLOW 11726 membrane and on the OPPO BAND GREEN 8003 membrane tested at the following three levels of equi-biaxial stretch ( $\lambda$ ): 1, 2, 3.

- Figure 15 reports the dielectric constant data acquired on the VHB 4905 membrane tested at the following four levels of equi-biaxial stretch ( $\lambda$ ): 3, 4, 5, 6.

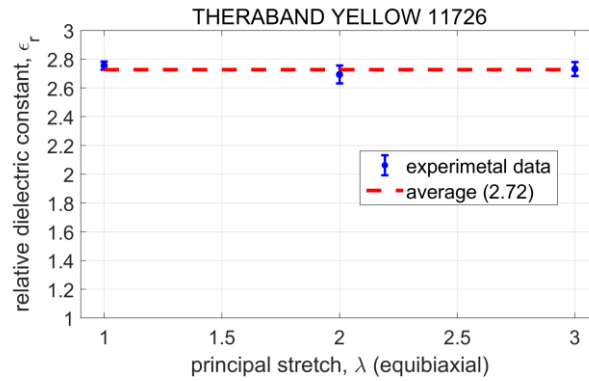


**Figure 13: Dielectric constant vs. stretch correlation for THERABAND YELLOW 11726**

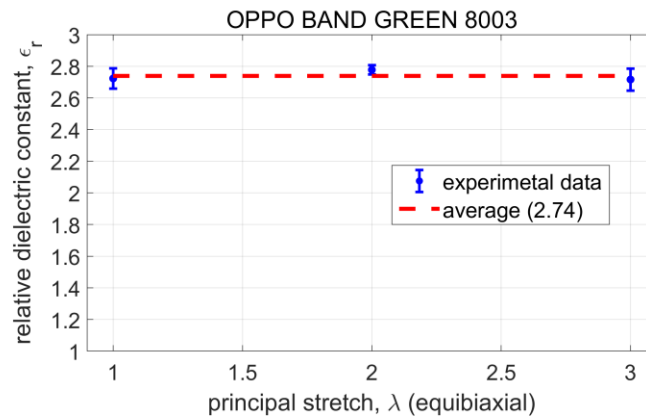


**Figure 14: Dielectric constant vs. stretch correlation for OPPO BAND GREEN 8003**

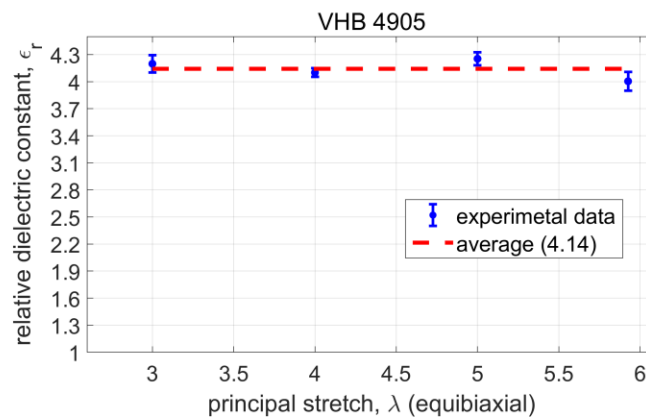


**Figure 15: Dielectric constant vs. stretch correlation for VHB 4905**

In the figures, blue dot markers represent the average over the three measurements performed on the three specimens tested at the same conditions, with the blue error bar representing their standard deviation. The red dashed line corresponds instead to the mean dielectric constant of the material, which is reported in Table 1, that is obtained by averaging all the measurements performed on a same material over the applied strain levels.

Overall, the results show:

- a rather negligible dependency of dielectric constant on applied strain for all of the considered materials;
- the average dielectric constants of THERABAND YELLOW 11726 and OPPO BAND GREEN 8003 are very similar, with the latter being slightly larger;
- the VHB 4905 is the material with highest dielectric constant.

As compared to other results existing in the literature, the findings obtained here for OPPO BAND GREEN 8003 are in line with those described in [24], which reports a dielectric constant  $\varepsilon = 2.8$ . However, this is not the case for the VHB 4905 membrane; in many papers, indeed, its thicker version (the VHB 4910) is quoted to have a dielectric constant that varies sensibly with strain. To comment more on this, Table 2 compares the values of dielectric constant estimated here for three stretch levels ( $\lambda = 3, 4, 5$ ) with those extracted from four different published papers [32,33,37,38]. Clearly, results are not consistent across the different works. This can be attributed to the following reasons:

- Formation of an air film between electrodes and tested specimen in the case of rigid electrodes that is due to the surface roughness of the membrane. This air film may reduce the measured value of capacitance, with the reduction typically increasing with specimen stretch, since the effective area of contact between electrode and membrane is likely to diminish with biaxial strain (since thinner portions of the membrane deform more than the thicker ones, the ratio between crest area and valley area of the surface roughness of the membrane is expected to decrease with strain).
- Influence of edge effects on the measured value of capacitance which, according to the standard ASTM D150 and as further detailed in [39], provides an error on the measured dielectric constant that increases as the diameter of the electrode decreases, as the height of the electrode increases and as the thickness of the membrane under test increases (thereby, as the stretch applied to a same virgin membrane decreases). As mentioned in Section 3.4, this effect should be negligible for the electrode arrangement considered here. However, this is less the case for the set-ups adopted in previous works, for which the ratio of fringing capacitance (estimated as per standard ASTM D150 and [39]) and measured capacitance can be as high as 10 % and dependent of the strain applied on the specimen.

	This paper VHB 4905 Carbon grease electrodes 80 mm diameter Test @ 20 Hz	Kofod et al. [33] VHB 4910 Planar metal + carbon black electrodes 30 mm diameter Test @ 1-10Hz	Wiessler et al. [37] VHB 4910 Cylindrical gold electrodes 25 mm diameter Test @ 100 Hz	Li et al. [38] VHB 4910 Rigid platinum electrodes Unknown diameter Unknown frequency	Tröls et al. [32] VHB 4910 Silver paste electrodes 14 mm diameter Test @ 1Hz
$\lambda = 3$	$\epsilon_r = 4.198$	$\epsilon_r \approx 4.55$	$\epsilon_r = 3.71$	$\epsilon_r \approx 3$	$\epsilon_r = 3.83$
$\lambda = 4$	$\epsilon_r = 4.101$	$\epsilon_r \approx 4.48$	$\epsilon_r = 3.34$	$\epsilon_r \approx 2.75$	$\epsilon_r \approx 3.6$
$\lambda = 5$	$\epsilon_r = 4.254$	$\epsilon_r \approx 4.48$	$\epsilon_r = 2.62$	$\epsilon_r \approx 2.5$	$\epsilon_r = 3.44$

**Table 2: Dielectric constant of VHB 4905 at different equi-biaxial stretches ( $\lambda$ ): this study vs existing literature. Values preceded by the symbol “ $\approx$ ” have been extrapolated from plots or data.**

In support to these arguments, it is worth recalling the results obtained in a preliminary work [30], where a thinner version of the natural rubber membrane considered here (namely, the OPPO BAND RED 8012) was tested with the cylindrical brass electrodes shown in Figure 2, which provided a permittivity significantly dependent on strain (thus, a response that is not consistent to the one measured here for the OPPO BAND GREEN 8003, which is made of the same natural rubber, with carbon grease electrodes that are 3.2 times larger in diameter).

### 3.5 Measurement of membrane stress-strain response

The experimental results of the tests conducted for assessing the stabilized stress-strain cyclic response of the considered DE membranes and its dependency on applied strain amplitude and strain rate are reported in Figures 16-21. In particular:

- Figures 16-18 report the stress-strain curves respectively for THERABAND YELLOW 11726, OPPO BAND GREEN 8003 and VHB 4905 membranes when tested at large stokes (namely, with a maximum deformation level equal to 90 % of the elongation at break limit of the considered material and a minimum deformation level corresponding to the value at null mechanical stress for the cycle performed at the smaller strain rate of  $0.004 \text{ s}^{-1}$ ).
- Figures 19-21 report the stress-strain curves respectively for THERABAND YELLOW 11726, OPPO BAND GREEN 8003 and VHB 4905 membranes when tested at intermediate stokes (namely with a reduced strain amplitude and with a deformation range adjusted so as to get the most effective response from the material, which compromises between minimal loss of tension during maximal electrical activation and reduced viscous losses during cyclical deformation).

In the figures, different line styles and colours are used to indicate experimental data acquired at different deformation rates,  $d\lambda_1/dt$ ; specifically: cyan circle markers for  $d\lambda_1/dt = 0.004 \text{ s}^{-1}$ , black solid line for  $d\lambda_1/dt = 0.08 \text{ s}^{-1}$ , dashed blue line for  $d\lambda_1/dt = 0.4 \text{ s}^{-1}$ , red dashed-dotted line for  $d\lambda_1/dt = 0.8 \text{ s}^{-1}$  and magenta dotted line for  $d\lambda_1/dt = 1.2 \text{ s}^{-1}$ .

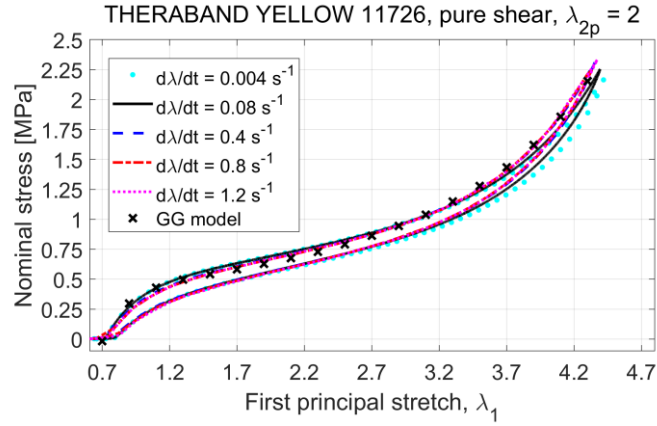


**Figure 16. Cyclic stress-strain response of a pure-shear specimen with transversal pre-stretch  $\lambda_{2p} = 2$  made of THERABAND YELLOW 11726 for large stroke: experimental data at different strain rates vs. Gent-Gent (GG) model fitting**

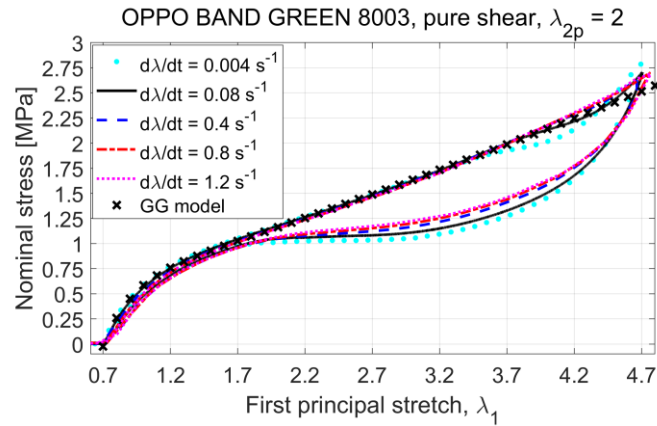


**Figure 17. Cyclic stress-strain response of a pure-shear specimen with transversal pre-stretch  $\lambda_{2p} = 2$  made of OPPO BAND GREEN 8003 for large stroke: experimental data at different strain rates vs. Gent-Gent (GG) model fitting**



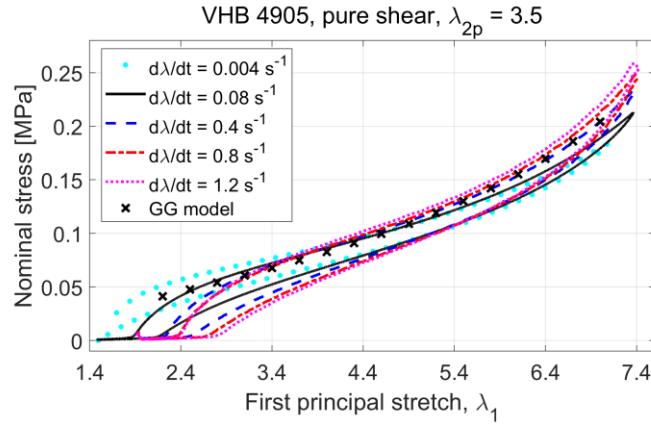


**Figure 18. Cyclic stress-strain response of a pure-shear specimen with transversal pre-stretch  $\lambda_{2p} = 3.5$  made of VHB 4905 for large stroke: experimental data at different strain rates vs. Gent-Gent (GG) model fitting**

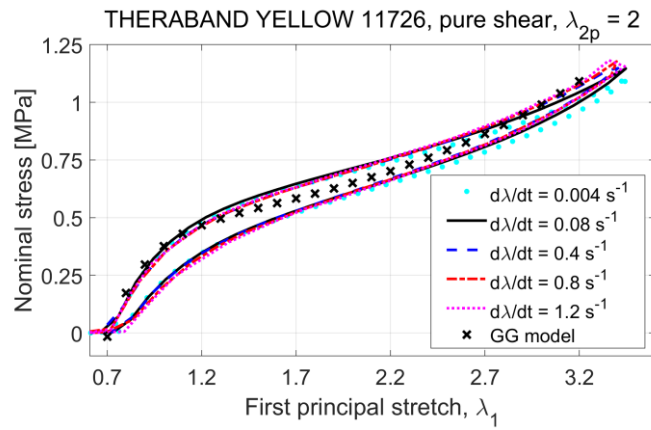


**Figure 19. Cyclic stress-strain response of a pure-shear specimen with transversal pre-stretch  $\lambda_{2p} = 2$  made of THERABAND YELLOW 11726 for intermediate stroke: experimental data at different strain rates vs. Gent-Gent (GG) model fitting**

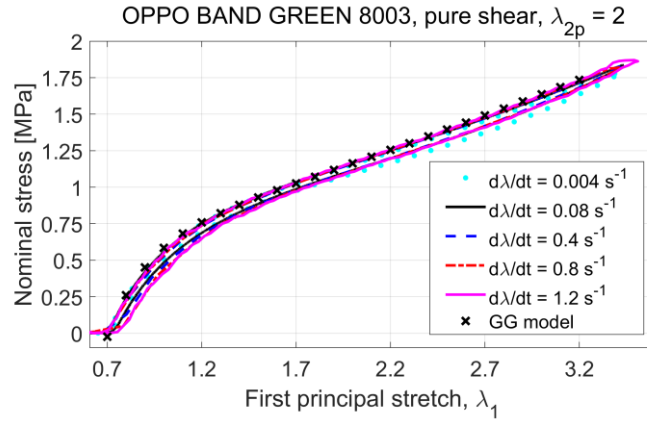


**Figure 20. Cyclic stress-strain response of a pure-shear specimen with transversal pre-stretch  $\lambda_{2p} = 2$  made of OPPO BAND GREEN 8003 with a transversal for intermediate stroke: experimental data at different strain rates vs. Gent-Gent (GG) model fitting**

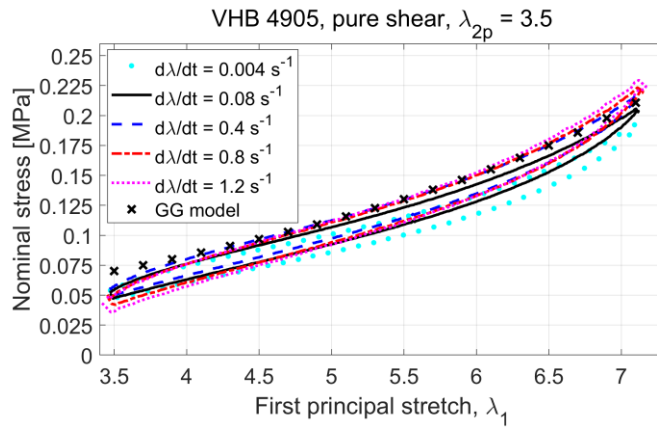


**Figure 21. Cyclic stress-strain response of a pure-shear specimen with transversal pre-stretch  $\lambda_{2p} = 3.5$  made of VHB 4905 for intermediate stroke: experimental data at different strain rates vs. Gent-Gent (GG) model fitting**

Overall, the results show:

- The stress-strain responses of the considered materials are all affected by hysteresis and viscosity, with the stresses being always higher during loading than during unloading. This indicates the presence of non-negligible mechanical dissipations. For a quantification, Table 3 summarizes the ratio between the mechanical energy lost in a cycle (namely, the area enclosed by the stress-strain curve) and the mechanical work spent to achieve maximal strain (namely, the area subtended by the loading curve over the entire deformation range) for all the tests reported in Figures 16-21. As it can be seen, for the considered materials, the percentage of energy lost in a cycle: 1) weakly depends on deformation speeds, with the only exception being the VHB 4905 tested at large strokes which exhibits an increase

over 50 % while changing the operating conditions from slow to fast rates; 2) weakly depends on deformation amplitudes, with the only exception being the OPPO BAND GREEN 8003 which exhibits an increase over 200 % while changing the operating conditions from intermediate to large strokes.

- The stress-strain response of VHB 4905 becomes stiffer as the strain rate increases, with this effect being more evident for the larger deformation amplitude. Such a behaviour indicates that VHB 4905 is significantly affected by visco-elasticity. This is not the case for the other two materials, which show very little dependency on strain rate, indicating that mechanical dissipations in THERABAND YELLOW 11726 and OPPO BAND GREEN 8003 are mostly due to visco-plasticity [42].
- The stress-strain response of VHB 4905 is softer by more than one order magnitude with respect to those of THERABAND YELLOW 11726 and OPPO BAND GREEN 8003, which are comparable although the latter is stiffer especially at smaller stretches (this can be seen by comparing Figures 19 and 20). The higher elastic stress values exhibited by THERABAND YELLOW 11726 and OPPO BAND GREEN 8003 reduce the chances of electrically-induced loss-tension, thereby increasing their operating limits; although they are likely to require the addition of external stiffness compensating mechanisms [43,44] to build practically usable devices.
- Although VHB 4905 is highly deformable, admitting for the considered pure-shear specimens a maximum longitudinal strain  $\lambda_{max} \approx 7.4$ , the strain range that can be exploited in practical applications is severely limited by mechanical dissipations. Indeed, the minimum longitudinal strain which needs to be used to prevent loss of tension due to visco-elasticity and visco-plasticity is:  $\lambda_{min} \approx 1.4$  for  $d\lambda_1/dt = 0.004 \text{ s}^{-1}$ ,  $\lambda_{min} \approx 1.9$  for  $d\lambda_1/dt = 0.08 \text{ s}^{-1}$ ,  $\lambda_{min} \approx 2.2$  for  $d\lambda_1/dt = 0.4 \text{ s}^{-1}$ ,  $\lambda_{min} \approx 2.4$  for  $d\lambda_1/dt = 0.8 \text{ s}^{-1}$  and  $d\lambda_1/dt = 1.2 \text{ s}^{-1}$ . The strain range for practical operations is instead much larger for the other two materials which, irrespective of the strain rate, admit:  $\lambda_{max} \approx 4.4$  and  $\lambda_{min} \approx 0.7$  for THERABAND YELLOW 11726;  $\lambda_{max} \approx 4.7$  and  $\lambda_{min} \approx 0.7$  for OPPO BAND GREEN 8003 (although, according to Figures 17 and 20, keeping  $\lambda_{max} \leq 3.5$  should be preferable for this natural rubber membrane to limit energy losses due to visco-plasticity).
- With the stretch limits given at the previous point, the following stretch ratios can be obtained:  $\lambda_{max}/\lambda_{min} \approx 5.3$  for the VHB 4905 deforming at  $d\lambda_1/dt = 0.004 \text{ s}^{-1}$  (significantly decreasing down to  $\lambda_{max}/\lambda_{min} \approx 3.9$  for  $d\lambda_1/dt = 0.08 \text{ s}^{-1}$  and to  $\lambda_{max}/\lambda_{min} \approx 3$  for  $d\lambda_1/dt \geq 0.8 \text{ s}^{-1}$ );  $\lambda_{max}/\lambda_{min} \approx 6.3$  for THERABAND YELLOW 11726 irrespective of the testing deformation rate;  $\lambda_{max}/\lambda_{min} \approx 6.7$  for OPPO BAND GREEN 8003 irrespective of the testing deformation rate, although keeping  $\lambda_{max}/\lambda_{min} \leq 5$  should be preferred for this natural rubber membrane to limit energy losses due to visco-plasticity (see Figures 17 and 20). This indicates that THERABAND YELLOW 11726 is the best suited for the realization of compact actuators and generators with large operating strokes.

		Deformation rate				
		0.004 s <sup>-1</sup>	0.08 s <sup>-1</sup>	0.4 s <sup>-1</sup>	0.8 s <sup>-1</sup>	1.2 s <sup>-1</sup>
THERABAND YELLOW 11726	Intermediate stroke	10.17	10.24	9.4	10.13	11.23
	Large stroke	11.9	10.27	8.99	8.72	11.18
OPPO BAND GREEN 8003	Intermediate stroke	4.79	3.89	3.53	4.33	5.16
	Large stroke	24.17	23.24	21.21	19.45	18.89
VHB 4905	Intermediate stroke	10.83	10.47	11.07	11.33	12.84
	Large stroke	12.36	11.9	14.64	16.70	18.95

**Table 3: Hysteresis loss (in % of the maximum stored elastic energy) in a cycle as function of strain rate and range of deformation: THERABAND YELLOW 11726 vs. OPPO BAND GREEN 8003 vs. VHB 4905.**

In summary, with a hysteretic loss in the order of 10% for a wide deformation range, the THERABAND YELLOW 11726 is the best all-rounder; OPPO BAND GREEN 8003 is the best alternative for applications that do not require extreme deformations; VHB 4905 is only suitable for applications that require low material stiffness.

To provide a model of the recorded mechanical response, the ideal assumptions of homogeneous pure-shear deformation with transversal pre-stretch equal to  $\lambda_{2p}$  and hyperelastic material behaviour according to the Gent-Gent (GG) hyperelastic model [45] are considered, which lead to the following equation for the nominal longitudinal stress,  $P_1$ , as function of the longitudinal stretch,  $\lambda_1$ ,

$$P_1 = \mu \frac{\lambda_1 - \lambda_1^{-3} \lambda_{2p}^{-2}}{1 + (3 - \lambda_1^2 - \lambda_{2p}^2 - \lambda_1^{-2} \lambda_{2p}^{-2})/J_m} + 2C_2 \frac{\lambda_1 \lambda_{2p}^2 - \lambda_1^{-3}}{\lambda_1^{-2} + \lambda_{2p}^{-2} + \lambda_1^2 \lambda_{2p}^2} \quad (7)$$

where the elastic moduli,  $\mu$  and  $C_2$ , and the chain extensibility limit,  $J_m$ , are constitutive material parameters. In the equation:

- the first contribution proportional to  $\mu$  describes the influence of the first strain invariant and has a form that is best suited to capture the material response at the larger strain levels;
- the second contribution proportional to  $C_2$  describes the influence of the second strain invariant and is included to improve the accuracy of the model at the smaller strain levels, which is required in multiaxial loading conditions that typically occur in DE applications. As a matter of fact, the term depending on  $C_2$  in the GG model becomes more significant with respect to that depending on  $\mu$  as the deformation state goes from uniaxial to bi-axial, and for pure-shear specimens the more the transversal pre-stretch is increased.

Fitting equation (7) to the loading curves of the large stroke experimental data acquired for each of the three materials at the intermediate strain rate of 0.4 s<sup>-1</sup> provides the values for  $\mu$ ,  $C_2$ , and  $J_m$  reported in Table 1, together with the modelled stress-strain responses represented with black cross markers in Figures 16-21.

Irrespective of the material, equation (7) is shown to capture very well not only the trend of the experimental data used for the fitting (see Figures 16-18) but also the stress-strain responses in the cycles performed at intermediate stoke amplitudes (see Figures 19-21). This is of utmost importance for design applications that require models capable to accurately predict the material behaviour in operating regimes that are different from those employed for parameter identification.

Worth to be mentioned: the model is only inaccurate in replicating the response of VHB 4905 for stretches smaller than 3.5. This is completely reasonable since in that range of deformation the behaviour of the material is highly affected by visco-elasticity and visco-plasticity that cannot be accounted by the model, which indeed neglects any mechanical dissipation.

The mechanical parameters reported in Table 1 highlight the importance of considering the influence of the second strain invariant on stress, which is often neglected in the modelling of DE materials. The moduli  $\mu$  and  $C_2$  are indeed of comparable magnitude for both THERABAND YELLOW 11726 and OPPO BAND GREEN 8003; the only exception is the VHB 4905 for which  $C_2 \approx 0$ . This makes it possible to precisely estimate the infinitesimal initial shear modulus of the material (namely,  $\mu_0 = \mu + 2C_2/3$  [45] which is a concise descriptor of the stiffness) as well as to accurately represent its elastic stress-strain response over the entire wide range of deformations. To quantify these benefits, fitting of the experimental stress-strain data of both styrenic and natural rubber bands has also been performed with the standard Gent model [24] (namely, equation (7) with  $C_2 = 0$ ), which yields:

- $\mu = 262.87$  kPa and  $J_m = 48.23$  for THERABAND YELLOW 11726, which underestimate the infinitesimal initial shear modulus  $\mu_0 = 328.18$  kPa given by the full GG model, and provide a worse fitting statistics that is characterized by a sum of squares due to error (SSE) and a root mean squared error (RMSE) that are 9.7 times and 3.1 times larger than those obtained with the full GG model;
- $\mu = 564.04$  kPa and  $J_m = 611521$  for the OPPO BAND GREEN 8003, which underestimate the infinitesimal initial shear modulus  $\mu_0 = 619.39$  kPa given by the full GG model (in addition to provide an extremely large value for the chain extensibility limit parameter), and provide a worse fitting statistics that is characterized by a SSE and a RMSE that are 25.5 times and 5 times larger than those obtained with the full GG model.

As compared to existing literature, fitting of experimental data acquired on OPPO BAND GREEN 8003 and VHB 4910 (the same material as the VHB 4905) specimens with the standard Gent model is performed in [24], which reports  $\mu = \mu_0 = 466$  kPa and  $J_m = 43$  for OPPO BAND GREEN 8003,  $\mu = \mu_0 = 52$  kPa and  $J_m = 114$  for the VHB 4910, and a rather good replication of the stress-strain data described therein. The values of these material parameters are notably different from those reported here. This is not surprising since the data fitting performed in [24] is based on experimental data acquired on specimens with different geometry (namely, uniaxial specimens rather than on transversally pre-stretched pure-shear specimens), which is likely to provide different material parameters [45]. Differently than in [31], which also suggests pure-shear testing, specimens

with a transversal pre-stretch larger than one (in particular,  $\lambda_{2p} = 2$  for THERABAND YELLOW 11726 and OPPO BAND GREEN 8003, and  $\lambda_{2p} = 3.5$  for VHB 4905) are employed here for the following two reasons:

- The resulting experimental data make the identification of the moduli  $\mu$  and  $C_2$  more unambiguous since, according to equation (7), the weight of the term multiplied by  $C_2$  compared to that multiplied by  $\mu$  increases as the transversal pre-stretch  $\lambda_{2p}$  is increased.
- The considered deformation states are likely to be closer to those experienced by the materials in practical DE transducers operating with large strain amplitudes or large pre-stretches.

#### 4. Discussion

This section provides a mixed qualitative-quantitative discussion on the performance of DETs that are based on the investigated materials in the context of applications that require the DE membrane to undergo large strain amplitudes as it occurs in actuators and generators with suitable static and dynamic stiffness compensation strategies [43,44,52,56,57,59,60].

The material performance is quantified in terms of a set of figures of merit (defined in Table 4) which are functions of the measured material parameters discussed so far. Such figures of merit can be combined with some more practical considerations and evaluations to provide a general comparison of the effectiveness of different materials for different applications.

We first consider some characteristic material parameters which solely depend on the material properties, regardless of the considered DET topology. Following that, the performance of the materials in combination with DETs operating in pure-shear is discussed.

A first relevant material parameter is the product of the dielectric constant  $\varepsilon$  ( $\varepsilon = \varepsilon_0 \varepsilon_r$ ) and the square of the dielectric strength  $E_{BD}^2$ . This parameter is (1) equal to the maximum electrostatic stress induced by the electric field,  $\sigma_e$  [46], and (2) proportional to the maximum energy density that can be converted by a DET [14]; thus, it is of key importance for both actuator and generator operations. As  $E_{BD}$  depends on the material stretch, typical ranges for each considered material are reported in Table 4. Despite having a lower dielectric constant, natural and styrenic rubber perform better than VHB 4905 in terms of the product  $\varepsilon E_{BD}^2$ , thanks to their larger dielectric strength. THERABAND YELLOW 11726 and OPPO BAND GREEN 8003 show similar dielectric performance, with the first one featuring slightly larger values due to its larger dielectric strength at large stretches.

	Variable	Expression & unit	THERA BAND YELLOW 11726	OPPO BAND GREEN 8003	VHB 4905
<i>Material parameters</i>	Maximum electrostatic stress	$\sigma_e = \varepsilon_0 \varepsilon_r E_{BD}^2$ [MPa]	0.15 - 2.0	0.17 - 1.6	0.12 - 1.0
	RC time constant	$\tau_{RC} = \varepsilon_0 \varepsilon_r / \kappa$ [s], in the range $E = 70\text{-}100$ MV/m	107.1 - 25.6	72.8 - 9.36	11.1 - 1.5
<i>Pure- shear DET performance</i>	Pre-stretch	$\lambda_{2p}$	2	2	3.5
	Min. stretch	$\lambda_{\min}$	0.70	0.70	1.4 - 2.4
	Max. stretch	$\lambda_{\max}$	4.4	4.7	7.4
	Stretch ratio	$\lambda_{\max} / \lambda_{\min}$	6.3	6.7	3 - 5.3
	Convertible energy density	$e_c = \varepsilon_0 \varepsilon_r \int_{\lambda_{\min}}^{\lambda_{\max}} \lambda_1^{-1} E^2 d\lambda_1$ [mJ/mm <sup>3</sup> ] with $E = \min \left\{ E_0 \left( \lambda_1 \lambda_{2p} \right)^{\frac{r}{2}}, \left( \frac{\lambda_1 P_1}{\varepsilon_0 \varepsilon_r} \right)^{\frac{1}{2}}, \left( \frac{\lambda_2 P_2}{\varepsilon_0 \varepsilon_r} \right)^{\frac{1}{2}} \right\}$	0.92	0.86	0.28 - 0.31
	Stored elastic energy density	$e_m = \int_{\lambda_{\min}}^{\lambda_{\max}} P_1 d\lambda_1$ [mJ/mm <sup>3</sup> ]	3.5	5.9	0.62
	Viscous energy density	$e_v = \text{Visc. loss} \times e_m$ [mJ/mm <sup>3</sup> ]	0.30 - 0.41	1.11 - 1.42	0.08 - 0.12
	Convertible- to-elastic energy ratio	$e_c / e_m$	0.26	0.14	0.50
	Viscous-to- convertible energy ratio	$e_v / e_c$	0.33 - 0.45	1.29 - 1.65	0.25 - 0.42

\*  $P_i$  is the nominal stress in the  $i$ -th principal direction ( $i=1,2$ )

**Table 4. Comparison of performance metrics for THERABAND YELLOW 11726, OPPO BAND GREEN 8003 and VHB 4905.**

A second relevant parameter is the electric time constant of the material,  $\tau_{RC} = \varepsilon_0 \varepsilon_r / \kappa$ . Any DET has a RC time constant (owing to the balance of DE layers capacitance and resistance) proportional to  $\tau_{RC}$ , regardless of the transducer's geometry. This parameter provides information on (1) the order of magnitude of the self-discharging time of a DET in the absence of a supplied current and (2) energy losses due to leakage currents

through the DE layers. In DE actuators, low values of the time-constant cause an increase of the supplied current (and, hence, of the energy consumption) which is however considered affordable in most DE actuator applications. In DE generators, this parameter is of greater relevance, as leakage current losses may even render generation impossible. In Table 4, we compare the variability ranges of  $\tau_{RC}$  for the three materials over typical operating electric fields (based on equation (6)). Natural and styrenic rubber show characteristic time-constants up to hundreds of seconds, while VHB 4905 has a time constant one order of magnitude lower (due to its large conductivity). The time-constants of the first two materials show that natural and styrenic rubber are, among others, promising options for low-frequency energy scavenging applications, like energy harvesting from ocean waves (whose frequency is in the range from 0.05 Hz to 0.2 Hz).

We hereby consider large-strain actuators and generators made of a DE membrane subject to pure-shear deformation, in which large strains can be obtained through the application of static or dynamic stiffness compensation strategies [43, 59, 18]. The pre-stretches and stretch ranges considered for the calculations (see Table 4) are the same as those used in large-stroke mechanical tests in Section 3.5. Despite the specific layout choice, the figures of merit presented in the following provide a rather general view of the different materials' potential in large-strain DE transducer applications.

We first compare the materials in terms of the useful energy density,  $e_c$ , that can be converted in a full-stroke cycle by the DET. This figure provides clear evidence of the applicability of a DE material for the construction of compact light-weight actuators and energy harvesters. Similarly to [14], in order to calculate the maximum convertible energy, we assume that the DET is free of charge during one half of the stroke (e.g., from the minimum to the maximum stretch) and electrically activated at the maximum feasible electric field during the rest of the cycle. The maximum applied electric field in each configuration is the minimum between the dielectric strength and the electric field which causes the material to lose tension (i.e., the stresses on the membrane plane to become zero). The dielectric strength is computed from equation (5), replacing  $\lambda$  with the average stretch ratio over the membrane surface directions.

For each material, the convertible energy density is in the range from 0.1 mJ/mm<sup>3</sup> to 1 mJ/mm<sup>3</sup>, with THERABAND YELLOW 11726 and OPPO BAND GREEN 8003 featuring similar energy density and performing considerably better than VHB 4905. This is due to the following reasons: 1) VHB 4905 has a lower value of the product  $\epsilon E_{BD}^2$ ; 2) the low elastic modulus of VHB 4905 strongly limits the maximum applicable electric field since the maximum field at which this material can operate without loosing tension is lower than the break-down field over the entire operating range.

A second relevant energetic figure is the elastic energy density,  $e_m$ , involved in a full deformation of the DET (from the minimum to the maximum stretch). In DE actuators, large values of the material elastic energy prevent the achievement of large actuation strains, unless static stiffness compensation strategies, such as non-linear spring biasing elements, are employed [43, 44, 52, 59, 60]. In energy harvesters, large amounts of elastic energy (namely, a very large material stiffness) are likely to cause a mismatch between harvester natural frequency and input source excitation frequency (namely, dynamic detuning), leading to the need for dynamic compensation strategies (such as increase in the harvester inertia, non-linear spring biasing elements, etc.)



[17,18]. Owing to their large elastic modulus, the deformation of THERABAND YELLOW 11726 and OPPO BAND GREEN 8003 requires significantly larger amounts of elastic energy compared to VHB 4905. OPPO BAND GREEN 8003, in turn, requires an elastic energy 1.8 times larger than THERABAND YELLOW 11726 to be fully stretched.

VHB 4905 presents the highest value of the ratio  $e_c/e_m$ , which means that this material can be easily employed to implement large-strain DE actuators without the need of adding stiffness compensation mechanisms (this feature allowed it to become a popular material for the implementation of large-strain actuator prototypes at laboratory scale; see for instance [58]). THERABAND YELLOW 11726 performs better than OPPO BAND GREEN 8003 in terms of the convertible-to-elastic energy ratio, mainly because of its lower elastic modulus, thus providing a more promising option for the development of large-strain DE actuators, most probably requiring suitable articulated or flexible frames [56, 57] and/or non-linear spring biasing compensating mechanisms [43, 44, 52, 59, 60].

Another energetic parameter describing a DET performance is the dissipated energy,  $e_v$ , due to viscous losses. In Table 4,  $e_v$  is approximated as the product of the experimental viscous loss (see Table 3 in Section 3.5) in large-stroke tests by the elastic energy density,  $e_m$ . A more accurate estimate of this figure might be obtained through an extensive characterisation of the visco-elastic and visco-plastic responses of the material [40,42]. Similarly to  $e_m$ , the dissipated energy density is maximum for OPPO BAND GREEN 8003 and minimum for VHB 4905, which are the stiffest and the softest materials respectively. THERABAND YELLOW 11726 and VHB 4905 feature comparable values of the ratio  $e_v/e_c$  of the dissipated energy over the useful convertible energy, with VHB 4905 performing slightly better. Although the percentage viscoelastic loss of THERABAND YELLOW 11726 is lower than that of VHB 4905 (see Table 3), the large amounts of elastic energy involved in the deformation of THERABAND YELLOW 11726 make viscous losses rather significant (in the range between 33 % and 45 %) compared to the convertible electro-mechanical energy. In contrast, OPPO BAND GREEN 8003 presents a very large value of the ratio  $e_v/e_c$  (over 100 %), due to the combination of a large elastic energy (compared to  $e_c$ ) and a large percentage of viscous loss at large stretches. In actuators made of this material, mechanical losses might in fact result in a complete dissipation of the supplied electrical energy input, preventing any useful mechanical energy output to be produced. In the operation as energy harvester, in turn, the large value of the ratio  $e_v/e_c$  is expected to lead to poor mechanical-to-electrical energy conversion efficiency, but still usable devices.

Finally, it is worth observing that, besides the figures of merit discussed in this work, the suitability of a DE material for a specific application depends on other technological/operational factors, in particular:

- The durability of a DE material subject to cyclic electro-mechanical loading. In practical applications, in order to achieve a target DET lifetime, the maximum applicable stretch and electric field might be significantly lower than the static limit values, leading to a substantial reduction in the achievable performance.

- The manufacturability of DET assemblies combining a selected DE material with stretchable electrodes. The possibility of implementing different types of compliant electrodes (such as conductive polymers or thin metallic films) on different DE substrates practically affects the deformation range achievable with a transducer and, hence, the performance.

In terms of these latter aspects, other materials appear to be promising for DE applications, in addition to those investigated in this article. The wide class of silicone-based elastomers [22], for example, is nowadays regarded as one of the most promising options for DETs. A wide set of scalable manufacturing procedures for silicone dielectric-electrode multi-layered assemblies have been proven [47-49], and cyclic lifetime assessments have shown promising results compared to other DEs [50,51].

## 5. Conclusions

This paper addresses the comprehensive electro-mechanical characterization of a styrenic rubber membrane, the elastic band THERABAND YELLOW 11726, along with those performed with the same experimental set-up and procedures on two well-known materials for dielectric elastomer transducer applications: the natural rubber band OPPO BAND GREEN 8003 and the double-sided adhesive acrylic tape VHB 4905 by 3M. Following the fitting of experimental data with constitutive models for both the electrical and mechanical responses, the identified material parameters are used to discuss the potentialities of the three considered materials for the development of dielectric elastomer actuators and generators operating at large levels of operating strain or in the presence of large pre-stretches.

Results from the mechanical characterization highlight the following:

- The dielectric strength of the three materials shows a significant dependency on stretch, which can be adequately captured by a power law, and is likely to be significantly affected by moisture.
- The electrical conductivity of the three materials shows a significant dependency on the electric field, which can be adequately captured by an exponential law, and seems to be rather independent of the strain.
- The dielectric constant of the three materials seems to be rather independent of the strain; this contradicts previous findings whose results might have been influenced by the specific testing conditions and procedures used for parameter estimation.
- The mechanical behaviour of the three materials is mostly affected by visco-plasticity (namely, rate-independent effects), with visco-elasticity (namely, rate-dependent effects) playing a significant role only for the VHB 4905 material.
- The stress-strain response of the three materials during loading can be adequately modelled by a hyper-elastic strain energy function in the Gent-Gent form, which includes the dependency of both first and second invariants of strain; neglecting the influence of the second invariant, as often done in the

literature, does not make it possible to accurately capture the material response under multi-axial loading conditions.

Comparison among the three materials provides the following indications:

- Owing to their larger energy density and electrostatic stress, and lower electric time constant, THERABAND YELLOW 11726 and OPPO BAND GREEN 8003 should be preferred over VHB 4905 for the realization of both large-strain actuators and generators whenever a large elastic stiffness is not an issue (for instance, when an external mechanical compensator behaving like a negative spring can be included);
- Owing to significant lower viscous losses at larger strain amplitudes, THERABAND YELLOW 11726 should be preferred over OPPO BAND GREEN 8003 especially in transducers requiring very long strokes;
- With a dielectric strength that is less sensitive to moisture, THERABAND YELLOW 11726 should be preferred over OPPO BAND GREEN 8003 for transducers working with fluids and/or operating in humid environments (examples are pumps, valves, micro-fluidic devices and ocean wave energy converters).
- VHB 4905 could be an option only for transducers operating at limited speeds and in applications where intrinsic material stiffness is an issue (for instance, when an external mechanical compensator behaving like a negative spring cannot be added). However, due to its low electrical time constant, limited reliability and reduced lifetime, this material seems to be applicable only for demonstrators and laboratory prototypes.

The constitutive models and the identified material parameters can be used for model-based analyses, optimal design and control of dielectric elastomer transducers subject to large strains made with the considered membranes. In this view, the results reported here will have to be complemented with findings on lifetime, reliability and manufacturing. The results of this paper may instead not be applicable to the study and development of transducer operating with small-strain amplitudes.

Despite being among the most promising materials for dielectric elastomer transducer applications, this study has not considered silicone elastomers since the carbon grease electrodes, which have been used here for the measurements of electrical conductivity and dielectric constant, are not chemically compatible with this material and the use of dissimilar electrodes would have made the experimental results rather difficult to compare.

## References

- [1] Carpi, F., De Rossi, D., Kornbluh, R., Pelrine, R.E. and Sommer-Larsen, P. eds.. Dielectric elastomers as electromechanical transducers: Fundamentals, materials, devices, models and applications of an emerging electroactive polymer technology. Elsevier (2011).
- [2] Carpi, F. ed.. Electromechanically active polymers. Springer, 2016.
- [3] Kornbluh, R. D., Pelrine, R., Pei, Q., Heydt, R., Stanford, S., Oh, S., Eckerle, J., “Electroelastomers: applications of dielectric elastomer transducers for actuation, generation, and smart structures,” in Proc. SPIE Vol. 4698, 254-270, 2002.
- [4] OHalloran, A., OMalley, F., McHugh, P., “A review on dielectric elastomer actuators, technology, applications, and challenges,” Journal of Applied Physics, 104(7), 071101-071101, 2008.
- [5] Flittner, K., Schlosser, M., Schlaak, H. F., “Dielectric elastomer stack actuators for integrated gas valves,” in Proc. SPIE Vol. 7976, 79761K-79761K, 2011.
- [6] Maffli, L., Rosset, S., Shea, H. R., “Zipping dielectric elastomer actuators: characterization, design and modelling”, Smart Materials and Structures, 22(10), 104013, 2013.
- [7] Heydt, R., Kornbluh, R., Eckerle, J., Pelrine, R., “Sound radiation properties of dielectric elastomer electroactive polymer loudspeakers,” in Proc. SPIE Vol. 6168, 61681M-61681M, 2006.
- [8] Matysek, M., Lotz, P., Schlaak, H. F., “Tactile display with dielectric multilayer elastomer actuators,” in Proc. SPIE Vol. 7287, 72871D, 2009.
- [9] Carpi, F., Frediani, G., Turco, S., De Rossi, D., “Bioinspired Tunable Lens with Muscle-Like Electroactive Elastomers,” Advanced Functional Materials, 21(21), 4152-4158, 2011.
- [10] Choi, H. R., Ryew, S., Jung, K. M., Kim, H. M., Jeon, J. W., Nam, J. D., Tanie, K., “Soft actuator for robotic applications based on dielectric elastomer: quasi-static analysis,” in IEEE International Conference on Robotics and Automation, Vol. 3, 212-3217, 2002.
- [11] Gu, G. Y., Zhu, J., Zhu, L. M., & Zhu, X., “A survey on dielectric elastomer actuators for soft robots”, Bioinspiration & biomimetics, 12(1), 011003, 2017.
- [12] O'Brien, B., Thode, J., Anderson, I., Calius, E., Haemmerle, E., Xie, S., “Integrated extension sensor based on resistance and voltage measurement for a dielectric elastomer,” in Proc. SPIE Vol. 6524, 652415-652415, 2007.
- [13] Pelrine, R., Kornbluh, R., Eckerle, J., Jeuck, P., Oh, S., Pei, Q., Stanford, S., “Dielectric elastomers: generator mode fundamentals and applications,” in Proc. SPIE Vol. Vol. 4329, 148-156, 2001.

- [14] Koh, S.J.A., Keplinger, C., Li, T., Bauer, S., Suo, Z., “Dielectric elastomer generators: How much energy can be converted?,” *Mechatronics, IEEE/ASME Transactions on* 16(1), 33–41, 2011.
- [15] Chiba, S., Waki, M., Kornbluh, R., Pelrine, R., “Innovative power generators for energy harvesting using electroactive polymer artificial muscles,” in *Proc. SPIE* 6927(1), 692715–692719, 2008.
- [16] Jean, P., Wattez, A., Ardoise, G., Melis, C., Van Kessel, R., Fourmon, A., Barrabino, E., Heemskerk, J., Queau, J.P., “Standing wave tube electro active polymer wave energy converter,” in *Proc. of SPIE Vol* 8340, 83400C–1, 2012.
- [17] Moretti, G., Papini, G. P. R., Righi, M., Forehand, D., Ingram, D., Vertechy, R., Fontana, M. “Resonant wave energy harvester based on dielectric elastomer generator” *Smart Materials and Structures*, 27(3), 035015, 2018.
- [18] Moretti, G., Rosati Papini, G. P., Daniele, L., Forehand, D., Ingram, D., Vertechy, R., Fontana, M., “Modelling and testing of a wave energy converter based on dielectric elastomer generators”, *Proceedings of the Royal Society A*, 475(2222), 20180566, (2019).
- [19] Pelrine, R., Kornbluh, R., Pei, Q., Joseph, J., “High-speed electrically actuated elastomers with strain greater than 100%”, *Science*, 287(5454), 836-839, 2000.
- [20] Michel, S., Zhang, X. Q., Wissler, M., Löwe, C., Kovacs, G., “A comparison between silicone and acrylic elastomers as dielectric materials in electroactive polymer actuators”, *Polymer international*, 59(3), 391-399, 2010.
- [21] Romasanta, L. J., López-Manchado, M. A., Verdejo, R., “Increasing the performance of dielectric elastomer actuators: A review from the materials perspective”, *Progress in Polymer Science*, 51, 188-211, 2015.
- [22] Madsen, F. B., Daugaard, A. E., Hvilsted, S., Skov, A. L., “The Current State of Silicone-Based Dielectric Elastomer Transducers”, *Macromolecular rapid communications*, 37(5), 378-413, 2016.
- [23] Jung, K., Lee, J., Cho, M., Koo, J. C., Lee, Y., Choi, H. R. “Development of enhanced synthetic elastomer for energy-efficient polymer actuators”, *Smart Materials and Structures*, 16(2), S288, 2007.
- [24] Kaltseis, R., Keplinger, C., Koh, S. J. A., Baumgartner, R., Goh, Y. F., Ng, W. H., Kogler, A., Tröls, A., Foo, C.C., Suo, Z., Bauer, S., “Natural rubber for sustainable high-power electrical energy generation”, *RSC Advances*, 4(53), 27905-27913, 2014.
- [25] Rosset, S., Shea, H. R., “Flexible and stretchable electrodes for dielectric elastomer actuators”, *Applied Physics A*, 110(2), 281-307, 2013.

- [26] Araromi, O. A., Rosset, S., Shea, H. R., “High-resolution, large-area fabrication of compliant electrodes via laser ablation for robust, stretchable dielectric elastomer actuators and sensors”, *ACS applied materials & interfaces*, 7(32), 18046-18053, 2015.
- [27] Low, S. H., Lau, G. K., “Bi-axially crumpled silver thin-film electrodes for dielectric elastomer actuators”, *Smart Materials and Structures*, 23(12), 125021, 2014.
- [28] Chen, B., Lu, J. J., Yang, C. H., Yang, J. H., Zhou, J., Chen, Y. M., Suo, Z., “Highly stretchable and transparent ionogels as nonvolatile conductors for dielectric elastomer transducers”, *ACS applied materials & interfaces*, 6(10), 7840-7845, 2014).
- [29] Yang, C., Suo, Z., “Hydrogel ionotronics”, *Nature Reviews Materials*, 1, 2018.
- [30] Vertechy, R., Fontana, M., Stiubianu, G., Cazacu, M., “Open-access dielectric elastomer material database”, in *Electroactive Polymer Actuators and Devices (EAPAD) 2014* (Vol. 9056, p. 90561R). International Society for Optics and Photonics, 2014.
- [31] Carpi, F., Anderson, I., Bauer, S., Frediani, G., Gallone, G., Gei, M., Graaf, C., Jean-Mistral, C., Kaal, W., Kofod, G., Kollosche, M., Kornbluh, R., Lassen, B., Matysek, M., Michel, S., Nowak, S. O’Brien, B., Pei, Q., Pelrine, R., Rechenbach, B., Rosset, S., Shea, H., “Standards for dielectric elastomer transducers”, *Smart Materials and Structures*, 24(10), 105025, 2015.
- [32] Tröls, A., Kogler, A., Baumgartner, R., Kaltseis, R., Keplinger, C., Schwödiauer, R., Bauer, S., “Stretch dependence of the electrical breakdown strength and dielectric constant of dielectric elastomers”, *Smart Materials and Structures*, 22(10), 104012, 2013.
- [33] Kofod, G., Sommer-Larsen, P., Kornbluh, R., Pelrine, R., “Actuation response of polyacrylate dielectric elastomers”, *Journal of intelligent material systems and structures*, 14(12), 787-793, 2003.
- [34] Gatti, D., Haus, H., Matysek, M., Frohnepfel, B., Tropea, C., Schlaak, H. F., “The dielectric breakdown limit of silicone dielectric elastomer actuators”, *Applied Physics Letters*, 104(5), 052905, 2014).
- [35] Zakaria, S., Morshuis, P. H., Benslimane, M. Y., Yu, L., Skov, A. L., “The electrical breakdown strength of pre-stretched elastomers, with and without sample volume conservation”, *Smart Materials and Structures*, 24(5), 055009, 2015.
- [36] Dissado, L.A., Fothergill, J.C., *Electrical degradation and breakdown in polymers* (Vol. 9). IET, 1992.
- [37] Wissler, M., Mazza, E., “Electromechanical coupling in dielectric elastomer actuators”, *Sensors and Actuators A: Physical*, 138(2), 384-393, 2007.
- [38] Li, B., Chen, H., Qiang, J., Zhou, J., “A model for conditional polarization of the actuation enhancement of a dielectric elastomer”, *Soft Matter*, 8(2), 311-317, 2012.

- [39] Woolley, D. E., "Edge correction in calculation of dielectric constant", *Journal of Testing and Evaluation*, 39(2), 140-149, 2010.
- [40] Chiang Foo, C., Cai, S., Jin Adrian Koh, S., Bauer, S., Suo, Z., "Model of dissipative dielectric elastomers", *Journal of Applied Physics*, 111(3), 034102, 2012.
- [41] Gisby, T. A., Xie, S. Q., Calius, E. P., Anderson, I. A., "Leakage current as a predictor of failure in dielectric elastomer actuators", in *Electroactive Polymer Actuators and Devices (EAPAD) 2010* (Vol. 7642, p. 764213). International Society for Optics and Photonics, 2010.
- [42] Lion, A., "A constitutive model for carbon black filled rubber: experimental investigations and mathematical representation", *Continuum Mechanics and Thermodynamics*, 8(3), 153-169, 1996.
- [43] Berselli, G., Vertechy, R., Vassura, G., Castelli, V. P., "Design of a single-acting constant-force actuator based on dielectric elastomers", *Journal of Mechanisms and Robotics*, 1(3), 031007, 2009.
- [44] Hodgins, M., York, A., Seelecke, S., "Experimental comparison of bias elements for out-of-plane DEAP actuator system", *Smart Materials and Structures*, 22(9), 094016, 2013.
- [45] Ogden, R. W., Saccomandi, G., Sgura, I., "Fitting hyperelastic models to experimental data", *Computational Mechanics*, 34(6), 484-502, 2004.
- [46] Suo, Z., "Theory of dielectric elastomers", *Acta Mechanica Solida Sinica*, 23(6), 549-578, 2010.
- [47] Rosset, S., Araromi, O. A., Schlatter, S., Shea, H. R., "Fabrication process of silicone-based dielectric elastomer actuators" *Journal of visualized experiments: JoVE*, (108), 2016.
- [48] Fasolt, B., Hodgins, M., Rizzello, G., Seelecke, S., "Effect of screen printing parameters on sensor and actuator performance of dielectric elastomer (de) membranes", *Sensors and Actuators A: Physical*, vol. 265, pp. 10-19, 2017.
- [49] McCoul, D., Rosset, S., Schlatter, S., Shea, H., "Inkjet 3D printing of UV and thermal cure silicone elastomers for dielectric elastomer actuators", *Smart Materials and Structures*, 26(12), 125022, 2017.
- [50] Yi, C., Agostini, L., Fontana, M., Moretti, G., Vertechy, R., "On the Lifetime Performance of a Styrenic Rubber Membrane for Dielectric Elastomer Transducers, in *ASME 2018 Conference on Smart Materials, Adaptive Structures and Intelligent Systems* (pp. V001T03A028-V001T03A028). American Society of Mechanical Engineers, 2018.
- [51] Chen, Y., Agostini, L., Moretti, G., Berselli, G., Fontana, M., Vertechy, R., "Fatigue life performances of silicone elastomer membranes for dielectric elastomer transducers: preliminary results", in *Electroactive Polymer Actuators and Devices (EAPAD) XXI* (Vol. 10966, p. 1096616). International Society for Optics and Photonics, 2019.

- [52] J.S Plante, S. Dubowsky, "On the performance mechanisms of dielectric elastomer actuators", *Sensors and Actuators A: Physical* vol. 137, n. 1, pp. 96-109, 2007.
- [53] K. Pope, A. Tews, M. Frecker, E. Mockensturm, N.C. Goulbourne, A.J. Snyder, "Dielectric elastomer laminates for active membrane pump applications", *Electroactive Polymer Actuators and Devices (EAPAD)*, Vol. 5385, International Society for Optics and Photonics, 2004.
- [54] L. Calabrese, G. Frediani, M. Gei, D. De Rossi, F. Carpi, "Active compression bandage made of electroactive elastomers". *IEEE/ASME Transactions on Mechatronics*, vol. 23, n. 5, pp. 2328-2337, 2018.
- [55] T.G. McKay, E. Calius, I.A. Anderson, "The dielectric constant of 3M VHB: a parameter in dispute", *Electroactive Polymer Actuators and Devices (EAPAD)*, Vol. 7287, International Society for Optics and Photonics, 2009.
- [56] R. Vertechy, G. Berselli, V. Parenti Castelli, G. Vassura, "Optimal design of lozenge-shaped dielectric elastomer linear actuators: mathematical procedure and experimental validation" *Journal of Intelligent Material Systems and Structures*, vol. 21, n. 5, pp. 503-515, 2010
- [57] G. Moretti, M. Fontana, R. Vertechy, "Parallelogram-shaped dielectric elastomer generators: Analytical model and experimental validation", *Journal of Intelligent Material Systems and Structures*, vol. 26, n. 6, pp. 740-751, 2015
- [58] Y.F. Goh, S. Akbari, T.V. Khanh Vo, S.J.A. Koh, "Electrically-induced actuation of acrylic-based dielectric elastomers in excess of 500% strain" *Soft robotics*, vol. 5, n. 6, pp. 675-684, 2018.
- [59] S. Hau, D. Bruch, G. Rizzello, P. Motzki, S. Seelecke, S., "Silicone based dielectric elastomer strip actuators coupled with nonlinear biasing elements for large actuation strains", *Smart Materials and Structures*, vol. 27, n. 7, p. 074003, 2018
- [60] P. Loew, G. Rizzello, S. Seelecke, "Permanent magnets as biasing mechanism for improving the performance of circular dielectric elastomer out-of-plane actuators", in *Electroactive Polymer Actuators and Devices (EAPAD)*, vol. 10163, p. 101630Y, 2017.
- [61] M. Hodgins, S. Seelecke, "Systematic experimental study of pure shear type dielectric elastomer membranes with different electrode and film thicknesses", *Smart Materials and Structures*, vol. 25, n. 9, p. 095001, 2016.
- [62] F. Förster-Zügel, L. Braisz, H.F. Schlaak, "Characterization of the dielectric breakdown strength of thin elastic films in various ambient media". In *2016 IEEE International Conference on Dielectrics (ICD)*, vol. 1, pp. 569-572, 2016



- [63] F. Förster-Zügel, T. Grotepaß, H.F. Schlaak, “Characterization of the dielectric breakdown field strength of PDMS thin films: Thickness dependence and electrode shape”, in *Electroactive Polymer Actuators and Devices (EAPAD)*, vol. 9430, p. 94300D, 2015.
- [64] D. Yurchenko, Z.H. Lai, G. Thomson, D.V. Val, R.V Bobryk, “Parametric study of a novel vibro-impact energy harvesting system with dielectric elastomer” *Applied energy*, vol. 208, pp. 456-470, 2017.
- [65] R. Panigrahi, S.K. Mishra, A.K. Srivastava, S. Basu, “Analysis, design, and implementation of an elastomer generator based energy harvesting scheme”, *IEEE Transactions on Industrial Electronics*, vol. 66, n. 5, pp. 3507-3517, 2018.
- [66] R. Vertechy, M. Fontana, “Electromechanical characterization of a new synthetic rubber membrane for dielectric elastomer transducers”, in *Electroactive Polymer Actuators and Devices (EAPAD) 2015 (Vol. 9430, p. 94300K)*. International Society for Optics and Photonics, 2015.